Boundary Layer Approximation using Thwaites and Head's Entrainment Method

Farras Arira (13619013), Terang B Brantas (13619074), Derren Audric (13619127), Hanna Millah (23622012)
Faculty of Mechanical and Aerospace Engineering
Institut Teknologi Bandung
Bandung, Indonesia

I. Introduction

Viscous-inviscid interaction in the boundary layer of an airfoil is important to determine the velocity and pressure distribution by including the effect of viscosity. But in the computational domain prespective, the formulas need to be adjusted using some method. The panel method is used as the inviscid solver because this method could measure the inviscid part up to the outer part of the airfoil boundary layer using singularity element, in this case source and vortex distribution. For the viscous handler, the solver for integral boundary layer equation using Thwaites method, this solver needs input from inviscid solver and able to calculate boundary layer parameters around the airfoil. There are some results that already conducted on the previous task.

From the obtained results, there are still errors when compared with the results from XFOIL. This error occurs in the simulation results found from the centre to the trailing edge of the airfoil. Since only the laminar viscous flow is modelled in this simulation, the simulation is still not able to simulate other phenomena such as transition, separation and turbulent flow. Some of the parameters change significantly when entering a different flow region, for example the skin friction coefficient jumps up when turbulent flow is reached and the displacement and momentum thickness increase significantly outside the laminar region. This phenomenon has an impact on the overall performance calculation of the airfoil, such as the drag coefficient. In order to improve the results, a turbulent flow model and accurate calculation of the transition location should be implemented. In this project, we use Head's Entrainment method to solve the turbulent boundary layer, and Michel method to determine the laminar-to-turbulent transition location.

This task will be divided into several section, the task structured as follows. Section 1 introduction. Section 2 discusses method to solve the inviscid flow. Section 3 discusses method to solve the viscous flow. Section 4 Laminar to Turbulent Transition Model. Section 5 explains about The Viscous Inviscid Interaction. Section 6 deals with validation and analysis of results. Section 7 deals with conclusions. Section 8 source code and the last references.

II. Inviscid Flow

A. Potential Flow

Panel method was developed based on potential flow, where the flow is assumed to have irrotational homentropic properties. In potential flow, there is a function Φ, called potential function, such that

$$\vec{V} = \vec{\nabla}\Phi \tag{1}$$

where $\vec{v}$ is vector field of velocity. Since the flow is irrotational or $\vec{\nabla} \times \vec{v} = 0$, using equation 1, the following equation could be obtained.

$$\nabla^2\Phi = 0 \tag{2}$$

Equation 2 is called the Laplace equation. This equation can be solved using the known boundary condition. Once the potential function Φ is known, the vector field of velocity can be obtained. The pressure coefficient C_p is then calculated by using the following equation below.

$$C_p = 1 - \frac{V(x,y)^2}{V_\infty^2} \tag{3}$$

Since the Laplace equation has the form of linear differential equation, any linear combination of the solution will also be the solution of the equation. Hence the Laplace equation can be solved by finding some elementary solutions. The example of such solutions are sources, vortices, doublets, etc. For the case of flow over airfoil, these elementary solutions are distributed along the airfoil surface and the flow tangency along the airfoil surface and Kutta condition are used as the boundary conditions.

B. Panel Method

There are many combination of elementary solution that can be used to formulate a panel method. However, one of the simplest and first truly practical method that was proposed by Hess and Smith, Douglas Aircraft, at 1966, uses the distribution of the sources and vortices elementary solutions, or mathematically written as

$$\Phi = \Phi_\infty + \Phi_S + \Phi_V \tag{4}$$

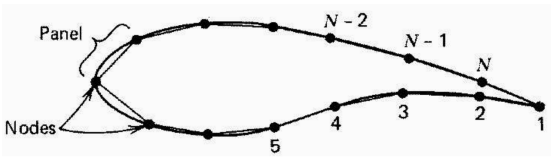

Fig. 1. Panel Method Discretization [1]

where Φ_∞ is freestream flow's potential function, Φ_S is the source distribution potential function and Φ_V is the vortex distribution potential function.

The potential function caused by source distribution along curve S at point P is formulated as

$$\Phi_S(P) = \int_S \frac{q(Q)}{2\pi} \ln r(P,Q) ds \tag{5}$$

where q is the strength of source, Q is any point in curve S and $r(P,Q)$ is the distance between point P and Q. The potential function caused by vortex distribution along the curve S at point P is formulate as

$$\Phi_V(P) = -\int_S \frac{\gamma(Q)}{2\pi} \ln r(P,Q) ds \tag{6}$$

where γ is the strength of vortex and θ is the angle between made by point P and Q.

Hess and Smith made an assumption that the the strength of the sources are varied along the body's surface, while the strength of vortices are constant. Besides that, to ease the calculation, the airfoil surface is discretized into a series of *panels*. The sequence of boundary point of each panel named in the clockwise direction, starting from the trailing edge as shown in Fig. 1. The control point for each panel is defined as the midpoint of the panel. Hence, the equation 4 can be extended as follows.

$$\begin{aligned}\Phi_{panel_i} =& \Phi_\infty + \sum_{j=1}^{N} \frac{q_j}{2\pi} \int_{panel_j} \ln r_{ij} ds_j - \\ & \frac{\gamma}{2\pi} \sum_{j=1}^{N} \int_{panel_j} \theta_{ij} ds_j \end{aligned} \tag{7}$$

where α is angle of attack and N is number of panels. The tangential and normal velocity on each panel can be computed by using the definition of potential flow as stated in equation 1.

$$\begin{aligned}V_{ni} =& V_\infty \sin\beta_i + \sum_{j=1}^{N} \frac{q_j}{2\pi} \int_{panel_j} \frac{\partial \ln r_{ij}}{\partial n_i} ds_j - \\ & \frac{\gamma}{2\pi} \sum_{j=1}^{N} \int_{panel_j} \frac{\partial \theta_{ij}}{\partial n_i} ds_j \end{aligned} \tag{8}$$

$$\begin{aligned}V_{ti} =& V_\infty \cos\beta_i + \sum_{j=1}^{N} \frac{q_j}{2\pi} \int_{panel_j} \frac{\partial \ln r_{ij}}{\partial t_i} ds_j - \\ & \frac{\gamma}{2\pi} \sum_{j=1}^{N} \int_{panel_j} \frac{\partial \theta_{ij}}{\partial t_i} ds_j \end{aligned} \tag{9}$$

where β is the angle between free stream and panel normal direction. The integral term is defined as an influence coefficient for each panel.

$$I_{ij} \equiv \int_{panel_j} \frac{\partial \ln r_{ij}}{\partial n_i} ds_j \tag{10}$$

$$J_{ij} \equiv \int_{panel_j} \frac{\partial \ln r_{ij}}{\partial t_i} ds_j \tag{11}$$

$$K_{ij} \equiv \int_{panel_j} \frac{\partial \theta_{ij}}{\partial n_i} ds_j \tag{12}$$

$$L_{ij} \equiv \int_{panel_j} \frac{\partial \theta_{ij}}{\partial t_i} ds_j \tag{13}$$

For the normal velocity, the contribution from source of a panel to itself is $q_j/2$ and from vortex is zero. For the tangential velocity, the contribution from source of panel to itself is zero and from vortex is $\lambda_j/2$. Hence, the equation. Hence the equation 9 and 8 can be rewritten as follows.

$$V_{ni} = V_\infty \sin\beta_i + \frac{q_i}{2} + \sum_{j=1, j\neq i}^{N} \frac{q_j I_{ij}}{2\pi} - \frac{\gamma}{2\pi} \sum_{j=1, j\neq i}^{N} K_{ij} \tag{14}$$

$$V_{ti} = V_\infty \cos\beta_i + \sum_{j=1, j\neq i}^{N} \frac{q_j}{2\pi} + \frac{\gamma_i}{2} - \frac{\gamma}{2\pi} \sum_{j=1, j\neq i}^{N} L_{ij} \tag{15}$$

The tangential velocity boundary condition and Kutta condition are respectively mathematically expressed as follows.

$$V_{ni} = 0 \qquad \text{for } i = 1, \ldots, N \tag{16}$$

$$V_{t1} = -V_{tN} \tag{17}$$

Substitute equation 14 to equation 16 and substitute equation 15 to equation 17, after some arrangements, the following equations are obtained.

$$-2\pi V_\infty \cos\beta_i = \pi q_i + \sum_{j=1, j\neq i}^{N} q_j I_{ij} - \gamma \sum_{j=1, j\neq i}^{N} K_{ij} \tag{18}$$

$$\begin{aligned}-2\pi V_\infty (\sin\beta_1 + \sin\beta_N) =& \sum_{j=1}^{N} q_j (J_{1j} + J_{Nj}) - \\ & \gamma \sum_{j=1}^{N} (L_{1j} + L_{Nj}) + 2\pi\gamma \end{aligned} \tag{19}$$

The system of equations above must be solved simultaneously to obtain the strength of sources and vortex of each panel. The matrix form of equation 18 and 19 is made to make the calculation easier.

$$Ax = b \tag{20}$$

where

$$A = \begin{bmatrix} \pi & I_{12} & \dots & -\sum_{j=1,j\neq 1}^{N} K_{1j} \\ I_{21} & \pi & \dots & -\sum_{j=1,j\neq 2}^{N} K_{2j} \\ \vdots & \vdots & \ddots & \vdots \\ I_{N1} & I_{N2} & \dots & \sum_{j=1,j\neq N}^{N} K_{Nj} \\ J_{N1} & J_{12}+JN2 & \dots & \sum_{j=1}^{N}(L_{1j}+L_{Nj})+2\pi \end{bmatrix}$$

$$x = \begin{bmatrix} q_1 \\ q_2 \\ \vdots \\ q_N \\ \gamma \end{bmatrix}$$

$$b = \begin{bmatrix} -2\pi V_\infty \cos\beta_1 \\ -2\pi V_\infty \cos\beta_2 \\ \vdots \\ -2\pi V_\infty \cos\beta_N \\ -2\pi V_\infty(\sin\beta_1 + \sin\beta_N) \end{bmatrix}$$

III. Viscous Flow

A. Boundary Layer Equations

Boundary layer equations initially developed by Ludwig Prantdl in 1904 by correct reduction of Navier-Stokes equations [2]. The reduced Navier-Stokes equations for boundary layer is as follows.

$$\frac{\partial \rho V_x}{\partial x} + \frac{\partial \rho V_y}{\partial y} = 0 \tag{21}$$

$$\rho\left(V_x\frac{\partial V_x}{\partial x} + V_y\frac{\partial V_x}{\partial y}\right) = -\frac{\partial p}{\partial x} + \frac{\partial}{\partial y}\left(\frac{\partial V_x}{\partial y}\right) \tag{22}$$

$$\frac{\partial p}{\partial y} = 0 \tag{23}$$

In order to solve the boundary layer equations for general cases, the approximate (integral) method can be used. The essential idea of theses method is to satisfy the momentum equation globally for the entire viscous layer. Being global, integral methods will allow to obtain information on global parameters such as the skin friction, displacement thickness, and momentum thickness. By utilizing the control volume analysis on the Navier-Stokes equations for boundary layer, the following von Karman integral equation is obtained.

$$\frac{d\theta}{dx} + (2\theta + \delta^*)\frac{dV_{in}}{V_{in}dx} = \frac{\tau_w}{\rho V_{in}^2} = \frac{C_f}{2} \tag{24}$$

where V_{in}, θ, δ^*, τ_w, and C_f denote inviscid flow velocity, momentum thickness, displacement thickness, skin friction at wall, and skin friction coefficient, respectively.

B. Thwaites Method

The Thwaites method is a modification and improvement of the integral parameter approximation method proposed by Pohlhausen [3], which was subsequently rewritten by Holstein & Bohlen (1940). The Thwaites method is derived by initially nondimensionalized using θ and V_{in}.

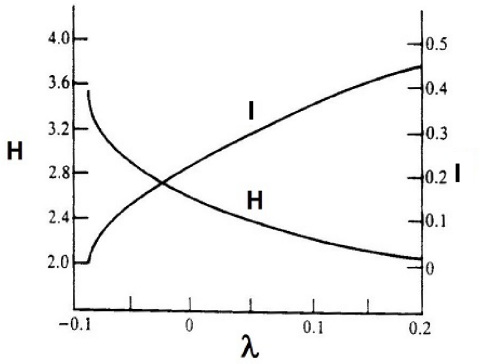

Fig. 2. Thwaites Correlation between λ, $l(\lambda)$, and $H(\lambda)$

$$\frac{V_{in}}{2\nu}\frac{d\theta^2}{dx} + (2+H)\frac{\theta^2}{\nu}\frac{dV_{in}}{dx} = \left(\frac{\theta}{V_{in}}\right)\left(\frac{\partial V_x}{\partial y}\right)_{y=0} \tag{25}$$

where $H = \dfrac{\delta^*}{\theta}$ is the shape factor. Defined that

$$\lambda = -\frac{\theta^2}{\nu}\frac{dV_{in}}{dx} \tag{26}$$

$$l = \left(\frac{\theta}{V_{in}}\right)\left(\frac{\partial V_x}{\partial y}\Big|_{y=0}\right). \tag{27}$$

Hence, the equation 25 can be rewritten as follows.

$$\frac{V_{in}}{\nu}\frac{d\theta^2}{dx} = 2((2+H)\lambda + l) \tag{28}$$

Based on the equation above, Thwaites argued that $l = l(\lambda)$ and $H = H(\lambda)$. Thwaites [4] draws the correlations from set of one-parameter functions with some experimental results and analytical calculations. He obtained the correlation shown by the Fig. 2. Hence,

$$\frac{V_{in}}{\nu}\frac{d\theta^2}{dx} = 2((2+H)\lambda + l) = F(\lambda) = 0.45 + 6\lambda \tag{29}$$

$$\frac{V_{in}}{\nu}\frac{d\theta^2}{dx} = 0.45 - 6\frac{\theta^2}{\nu}\frac{dV_{in}}{dx} \tag{30}$$

which integrates to

$$\theta^2 = \frac{0.45\nu}{V_{in}}\int_0^x V_{in}(x')^5 dx'. \tag{31}$$

It can be concluded the procedure to analyze boundary layer using Thwaites method is as follows.

1) Calculate momentum thickness θ using equation 31.
2) Calculate parameter λ using equation 26.
3) Calculate parameter l and H using known correlation shown in Fig. 2.
4) Calculate displacement thickness δ^* from H and θ.
5) Calculate friction coefficient using $C_f = \dfrac{2\nu}{V_{in}\theta}l$.

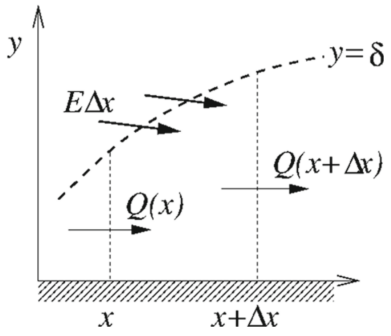

Fig. 3. Head's Entrainment Concept [8]

C. Head's Entrainment Method

Midway through the 1950s, M.R. Head, a flight lieutenant from World War II who was born in New Zealand [5], was researching boundary layers at the University of Cambridge (UK) from both an experimental and theoretical (calculative) perspective [6] [7]. He was interested in developing flow models suitable for engineering purposes in the latter case. He gathered a lot of data from numerous boundary layer experiments up to this point, or what is known as "big data" in modern parlance.

Head provides these data in a large number of graphs containing multiple variables in his report from September 1958 for the Aeronautical Research Council [7]. He hoped to discover a "magic" pattern between the variables that may be valuable for mankind. Evidently dissatisfied with what he discovered, he made the decision to create a new variable. He hypothesized that the boundary layer's entrainment would be crucial and, more importantly, universal.

In Fig. 3, Head's entrainment concept is schematized. He began by developing a new shape function $H_{\delta-\delta^*}$, based on $\delta - \delta^*$:

$$H_{\delta-\delta^*} \equiv \frac{\delta - \delta^*}{\theta} \tag{32}$$

The shape function $H_{\delta-\delta^*}$ is related to the mass transport $Q(x)$ per cross section, as shown by the Fig. 3.

$$Q \equiv \int_0^\delta u dy = U(\delta - \delta^*) = U\theta H_{\delta-\delta^*} \tag{33}$$

By the conservation law of mass, a mass influx from outside the boundary layer must make up for the variation of Q across a distance x. The entrainment E (per unit of length) is what is meant by this.

$$E \equiv \frac{dQ}{dx} = \frac{d}{dx}[U(\delta - \delta^*)] = \frac{d}{dx}(U\theta H_{\delta-\delta^*}) \tag{34}$$

By connecting these quantities, two assumptions were made by Head:

1) Assumption 1 : $\frac{E}{U}$ is function of only $H_{\delta-\delta^*}$.

$$\frac{E}{U} = F(H_{\delta-\delta^*}) \tag{35}$$

2) Assumption 2 : $H_{\delta-\delta^*}$ is a function of only H.

$$H_{\delta-\delta^*} = H_{\delta-\delta^*}(H) \tag{36}$$

In addition, Head Assumed that the skin friction on turbulent followed the impirical formula proposed by Ludwig and Tillman:

$$C_f = \frac{0.246}{10^{0.678H} R_\theta^{0.268}} \tag{37}$$

$$R_\theta = \frac{V_{in}\theta}{\nu} \tag{38}$$

Head then fitted the experimental data to the presupposed functional relations [9] [10]. The functional relation that he found based on his assumption is as follows.

$$\frac{E}{U} = F(H_{\delta-\delta^*}) = \frac{0.0306}{(H_1 - 3.0)^0.6169} \tag{39}$$

$$H_{\delta-\delta^*} = H_{\delta-\delta^*}(H) = 3.0445 + \frac{0.8702}{(H - 1.1)^1.2721} \tag{40}$$

By using Von-Karman equation 24, with known inviscid velocity, the turbulent boundary layer properties can be calculated by using additional equations 39, 40, and 37.

IV. Laminar-to-Turbulent Transition Model

The laminart-to-turbulent trnasition point should be determinet to separate laminar and turbulent flow. It is due to different method used to solve the boundary layer equation, where Thwaites method used for laminar flow while Head's Entrainment method used for turbulent flow.

There are various mathematical models that have been proposed to model the laminar-to-turbulent transition in boundary layer. Some of these models are the Granville method, The Michel method, the Jaffe method, and the Wazzen method [11]. It is found that the Michel method is extreamely easy to implement but also provides accurate solutions. Hence, in this project, the Michel method is used to model the transition phenomena in the boundary layer.

The Michel method was proposed by Michel in 1952. This method was in the form of a correlation based on the local values of momentum thickness and position. By using boundary layer equation, the momentum thickness θ is obtained, the transition occurs when at some point we strike Michel's "transition line" [11].

$$Re_{\theta,tr} \equiv \frac{U_{in}(x)\theta(x)}{\nu} = 2.9 Re_{x,tr}^{0.4} \tag{41}$$

V. The Viscous-Inviscid Interaction

Viscous-inviscid interaction is a coupling method between inviscid flow and viscous flow calculations. This coupling is important since boundary layer displacement affects the inviscid flow. To account for the displacement effect, it is therefore necessary to ensure the matching of normal velocities in addition to the matching of tangential velocities. By using

continuity equation, the boundary condition for inviscid flow in order to account the displacement effect is as follows.

$$V_n(y=0) = \frac{d}{dx}(V_{in}\delta^*) \tag{42}$$

The normal velocity $V_n(y=0)$ is often called transpiration velocity.

The coupling method based on the transpiration velocity is as follows.

1) The invisvid flow is calculated with boundary condition

$$V_n = 0 \quad \text{along the surface of body}$$

2) The boundary layer is calculated which provides the displacement thickness distribution $\delta^*(x)$
3) The inviscid flow is recomputed with boundary condition

$$V_n = \frac{d}{dx}(V_{in}\delta^*) \quad \text{along the surface of body}$$

4) Return to step 2. until the result is convergent.

The panel method is used for the inviscid flow analysis, thus the transpiration velocity boundary condition is taken in the formulation of the panel method. Since the transpiration velocity is normal velocity located along the surface of body, it can be substituted in equation 18.

$$2\pi V_{trp,i} - 2\pi V_\infty \cos\beta_i = \pi q_i + \sum_{j=1, j\neq i}^{N} q_j I_{ij} - \gamma \sum_{j=1, j\neq i}^{N} K_{ij} \tag{43}$$

where $V_{trp,i}$ is the transpiration velocity at panel i. Hence the new matrix b in equation 21 is rewritten as follows.

$$b = \begin{bmatrix} 2\pi V_{trp,1} - 2\pi V_\infty \cos\beta_1 \\ 2\pi V_{trp,2} - 2\pi V_\infty \cos\beta_2 \\ \vdots \\ -2\pi V_\infty(\sin\beta_1 + \sin\beta_N) \end{bmatrix} \tag{44}$$

The numerical algorithm of the viscous-inviscid interaction is shown by the Fig. 4.

VI. Results Validation

Results and validation are conducted by comparing the developed Thwaites with Head Entrainment Method result with the XFOIL result. The validation is conducted by variating the airfoil and freestream Reynold's Number. Such that, the validation is conducted for 6 cases, which are thin airfoil, thick airfoil, cambered airfoil, High Reynold Number, Low Angle of Attack and High Angle of Attack. Generally, in most cases, the present solver result is relatively the same as the XFOIL result. The differences occur in the area beyond the separation point which the present solver cannot accurately capture the phenomenon itself (detached flow). However, compared with the previously developed viscous solver, the present solver is capable to capture the turbulence regime before the separation occurs.

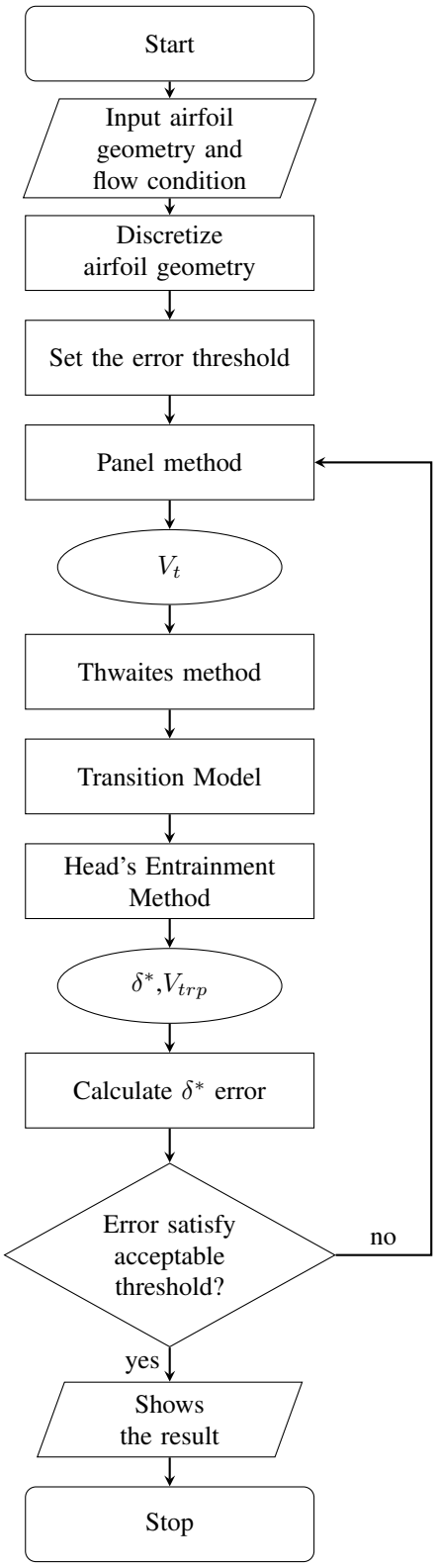

Fig. 4. Viscous-Inviscid Algorithm

A. Thin Airfoil

For the Thin Airfoil cases, the analyzed airfoil is NACA0008 with Re 1.3×10^6. Since using a symmetric airfoil with a zero angle of attack, the result at the upper and lower surfaces will be the same. In this case, the separation point is relatively close to the trailing edge as seen in Fig. 5. It can be seen that the transition point location relative to the airfoil chord is the same which is a consequence of the symmetric airfoil. At most of the airfoil surface, the present solver result for pressure distribution (Fig. 6) and momentum thickness (Fig. 8) is not significantly different from the XFOIL result. However, the displacement thickness (Fig. 7) and friction coefficient (Fig. 9) are slightly different compared with the XFOIL result at the area after the transition point.

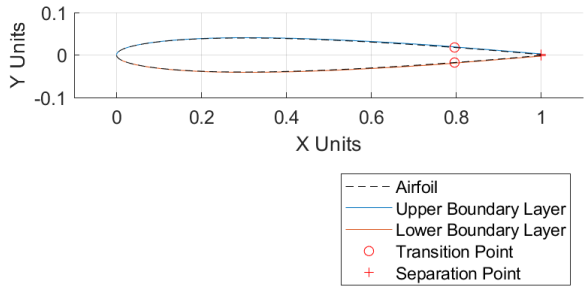

Fig. 5. Boundary Layer Displacement on NACA0008

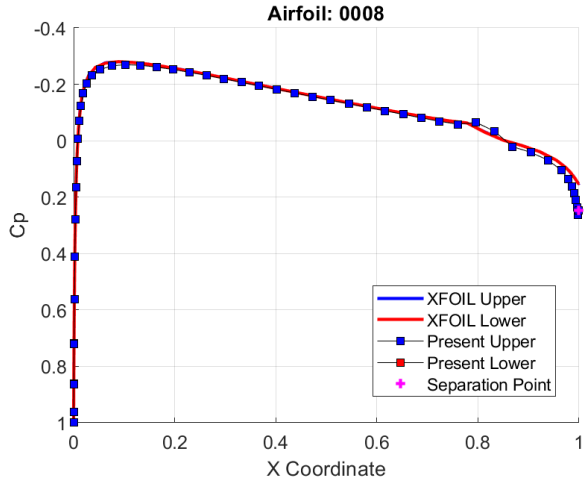

Fig. 6. Pressure Distribution on NACA0008

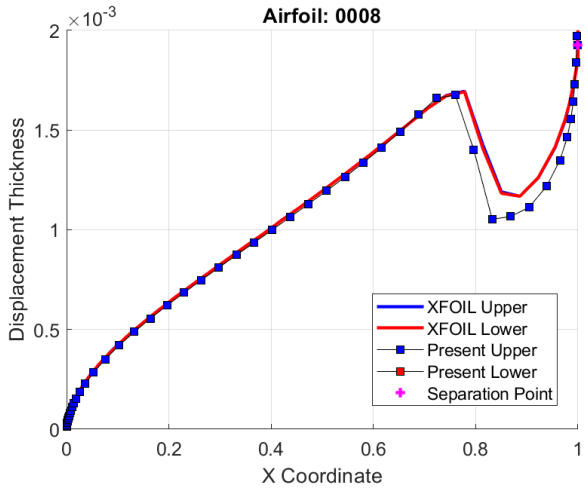

Fig. 7. Displacement Thickness on NACA0008

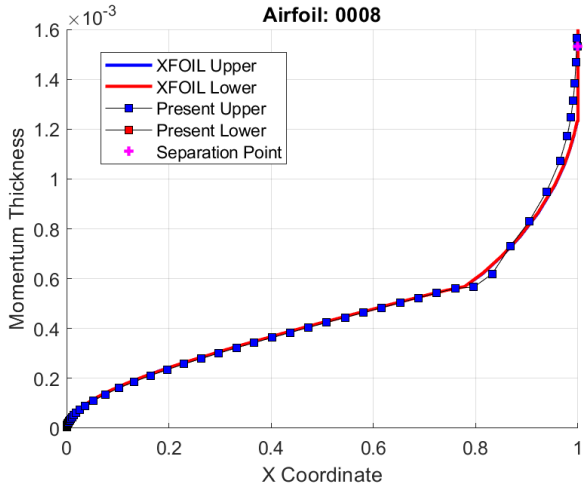

Fig. 8. Momentum Thickness on NACA0010

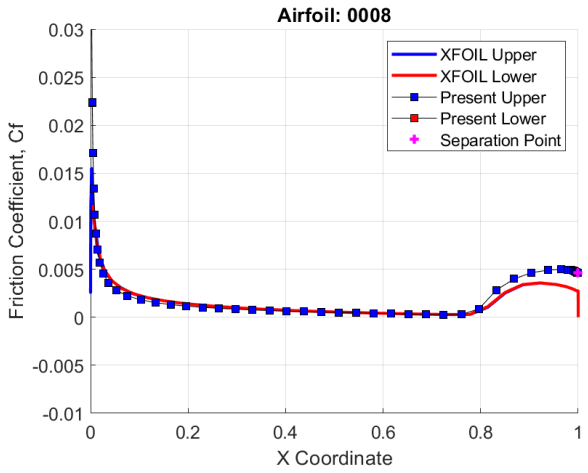

Fig. 9. Friction Coefficient Distribution on NACA0010

Those conditions cause a relatively high error in the calculated drag coefficient and a small error in the lift coefficient as

shown in Table I. The error in the drag coefficient is mainly caused by the friction coefficient differences in the area beyond the transition point which the present solver result is higher than the XFOIL result.

TABLE I
AERODYNAMIC COEFFICIENT COMPARISON OF NACA0008

parameters	present	XFOIL	error
lift coefficient, c_l	0.000141	0.000100	0.000%
drag coefficient, c_d	0.004228	0.003830	10.3%

B. Thick Airfoil

In this case, the thick airfoil, NACA0015, is used with Re 1.3×10^6. The significant difference from the previous Thin Airfoil case is the separation point that occur earlier as shown in Fig. 5. The general performance of the present solver is relatively the same as the thin airfoil result. Compared to the XFOIl result, the present solver gives relatively the same result for pressure coefficient (Fig. 6) and momentum thickness (Fig. 8) and slightly different in friction coefficient (Fig. 9) and displacement thickness (Fig. 7).

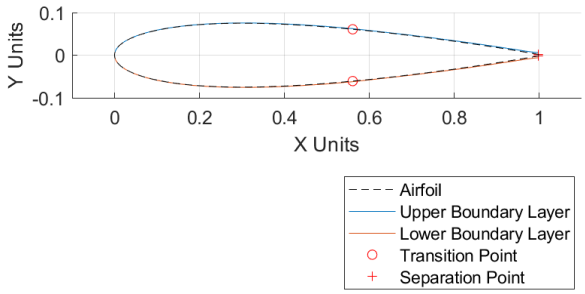

Fig. 10. Boundary Layer Displacement on NACA0015

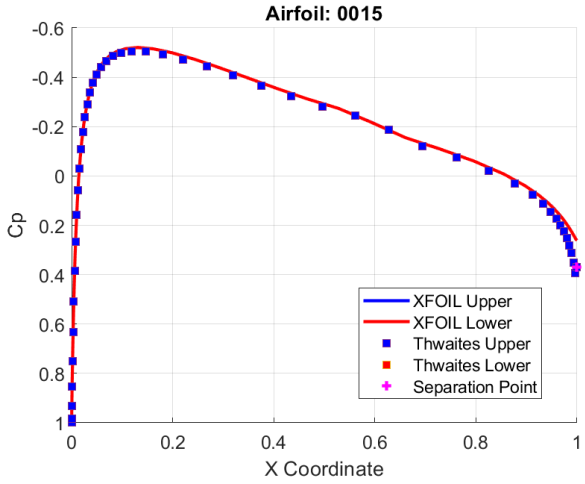

Fig. 11. Pressure Distribution on NACA0015

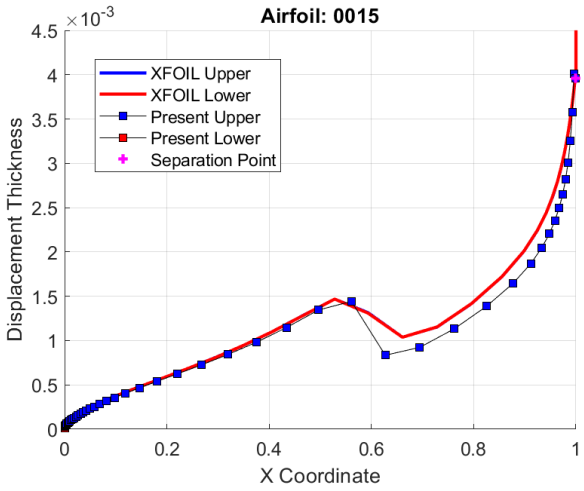

Fig. 12. Displacement Thickness on NACA0015

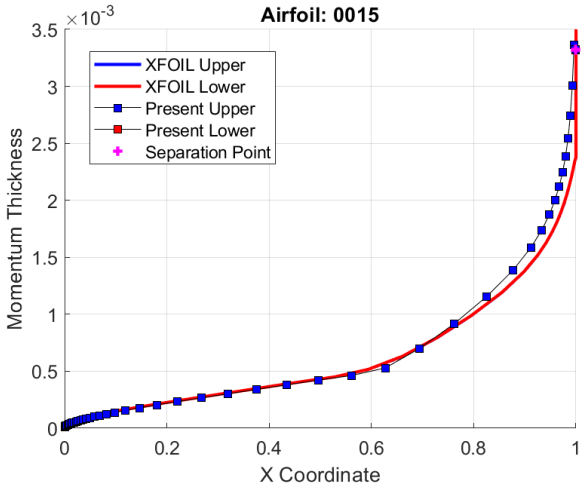

Fig. 13. Momentum Thickness on NACA0015

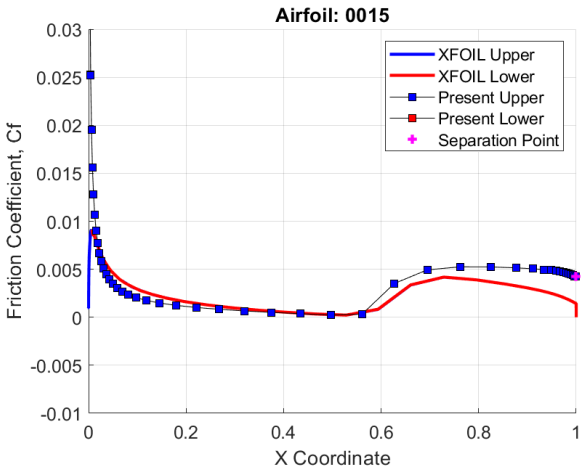

Fig. 14. Friction Coefficient Distribution on NACA0015

However, as seen in Table II, the resulting drag coefficient error is lower than in the thin airfoil case while the lift

coefficient error remains the same. This small error is caused by the difference in the value of the friction coefficient covered by the difference in the value of the pressure coefficient. As seen in Fig. 11, the pressure coefficient value after the transition point is slightly lower than the XFOIl result while the friction coefficient value in the Fig. 14 is higher than the XFOIL result at the area beyond the transition point.

TABLE II
AERODYNAMIC COEFFICIENT COMPARISON OF NACA0015

parameters	present	XFOIL	error
lift coefficient, c_l	0.00000	0.000000	0.000%
drag coefficient, c_d	0.005949	0.005800	2.6%

C. Cambered Airfoil

In this validation, the cambered airfoil, NACA 6419, is used with Re 1.3×10^6. Different from the previous cases, in this case, the transition point at the upper and lower surface is located at a different location relative to the airfoil chord as seen in Fig. 15. Another consequence is the resulting value in the upper and lower surface will be different. The resulting pressure distribution (Fig. 16) is relatively the same as the XFOIL result. However, the significant difference occurs in the Displacement Thickness result (Fig. 17), Momentum Thickness result (Fig. 18), and the Friction Coefficient result (Fig. 19). The differences mainly occur in the lower section of the airfoil where the transition point occurs very early. However, the upper surface result has a relatively smaller difference.

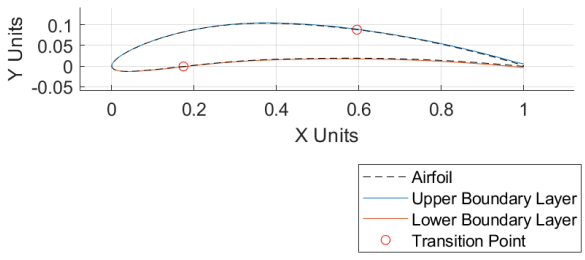

Fig. 15. Boundary Layer Displacement on NACA6419

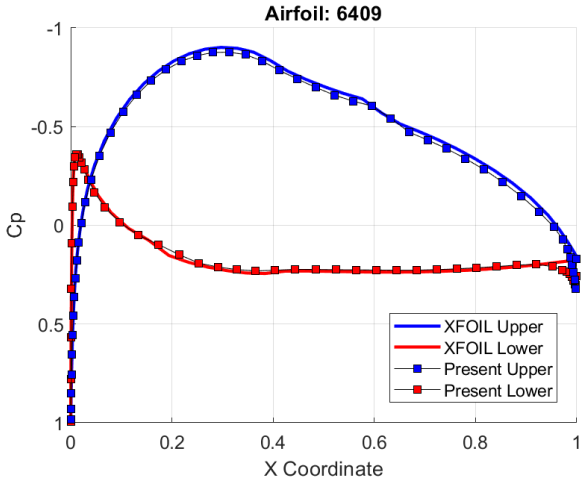

Fig. 16. Pressure Distribution on NACA6419

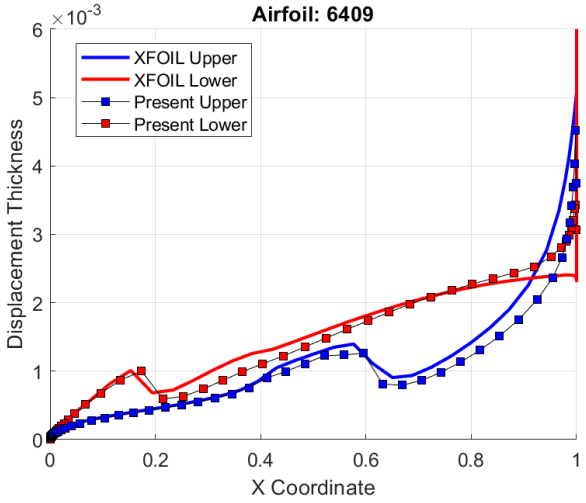

Fig. 17. Displacement Thickness on NACA6419

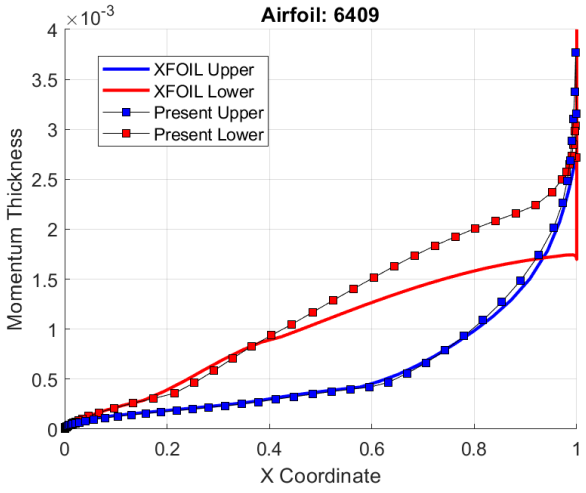

Fig. 18. Momentum Thickness on NACA6419

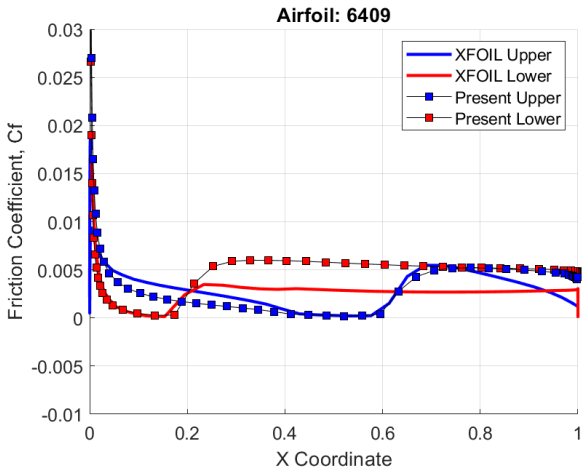

Fig. 19. Friction Coefficient Distribution on NACA6419

The resulting lift and drag coefficient has an error compared with previously symmetric case as seen in Table III. The lift coefficient has a low error compared with the XFOIL result while the drag coefficient has a relatively high error. The high error in the drag coefficient is due to the cumulative result of the error in the friction coefficient on the lower surface.

TABLE III
AERODYNAMIC COEFFICIENT COMPARISON OF NACA6419

parameters	present	XFOIL	error
lift coefficient, c_l	0.676216	0.699800	3.4%
drag coefficient, c_d	0.007569	0.006750	12.3%

D. High Reynolds Number

In this case, the selected airfoil is the symmetric airfoil (NACA0012) with a zero angle of attack and Re 2.0×10^7. However, the used freestream Reynold's Number is higher than in previous cases. The direct consequence of the high Reynold's Number is the transition point that occurs earlier even compared with the thicker airfoil. In this case, the transition point occurs around the maximum thickness of the airfoil as shown in Fig. 20. However, the general performance of the present solver is different than in previous cases. The pressure (Fig. 21) distribution remains the same compared with the XFOIl result. However, in this case, the displacement thickness (Fig. 22) result has relatively the same value as the XFOIL result. The differences only occur in the small area around the transition point. Meanwhile, the momentum thickness result (Fig. 23) has significant differences at the area beyond the transition point. However, the friction coefficient result (Fig. 24) remains the same as before, with a difference at the area beyond the transition point.

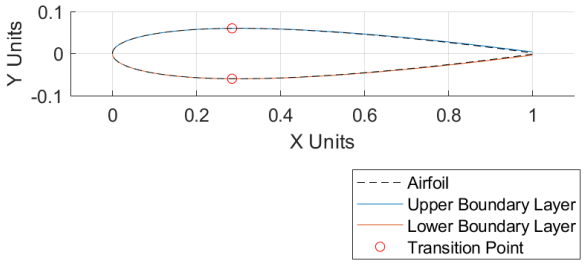

Fig. 20. Boundary Layer Displacement on NACA0012 with High Reynolds Number

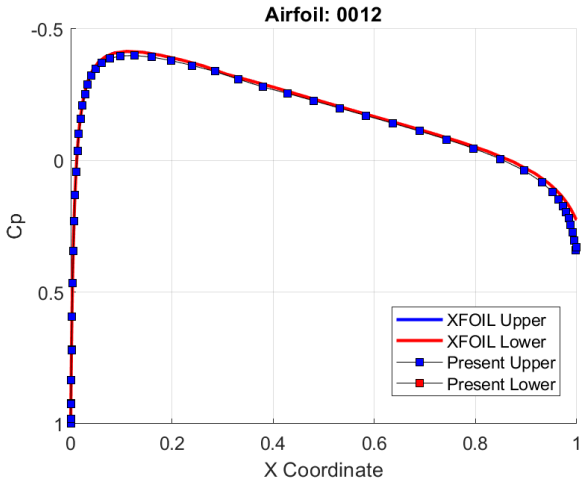

Fig. 21. Pressure Distribution on NACA0012 with High Reynolds Number

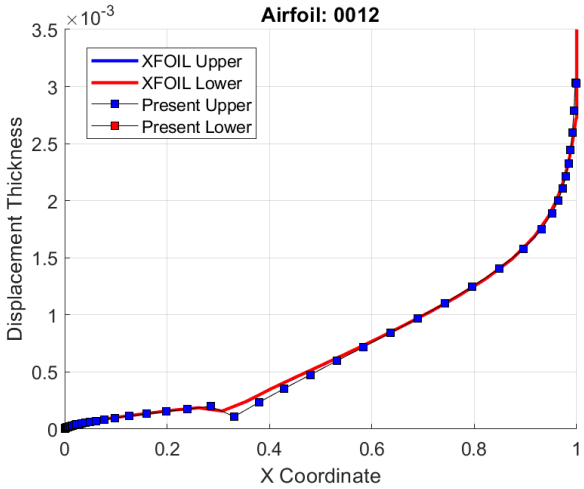

Fig. 22. Displacement Thickness on NACA0012 with High Reynolds Number

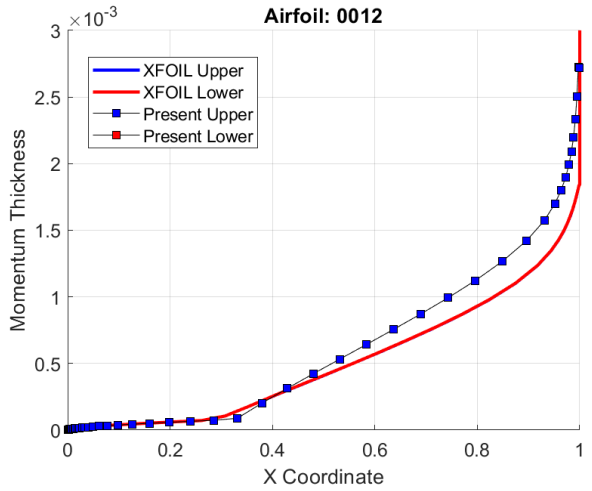

Fig. 23. Momentum Thickness on NACA0012 with High Reynolds Number

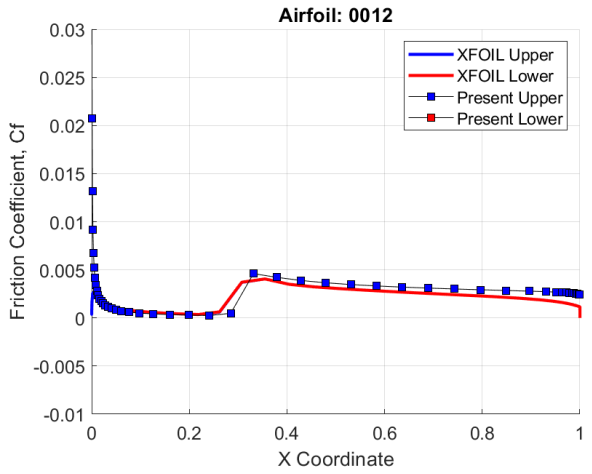

Fig. 24. Friction Coefficient Distribution on NACA0012 with High Reynolds Number

Although the friction coefficient differences are relatively small compared with the two previous cases, the resulting drag coefficient error is higher as seen in Table IV. This is due to the differences occurring in a longer area which cumulated in drag coefficient calculation.

TABLE IV
AERODYNAMIC COEFFICIENT COMPARISON OF NACA0012 ON HIGH REYNOLDS NUMBER

parameters	present	XFOIL	error
lift coefficient, c_l	0.000000	0.000000	0.0%
drag coefficient, c_d	0.005579	0.004920	13.4%

E. Low Angle of Attack

In this section the used airfoil remains the same, NACA0012, with a $1\,\mathrm{deg}$ angle of attack and Re 1.3×10^6. Since the angle of attack is not zero, the transition point will not occur in the same position relative to the chord as seen in Fig 25. It can be seen from figure 27, 28, 26, 29, the result of the present method is in good agreement with the XFOIL result.

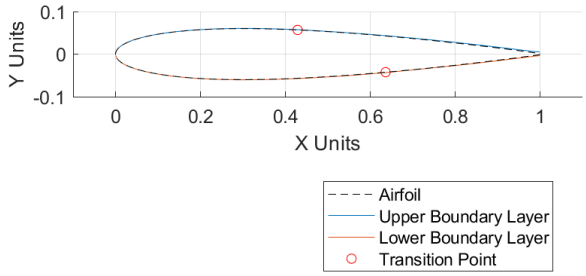

Fig. 25. Boundary Layer Displacement of NACA0012 on Low Angle of Attack

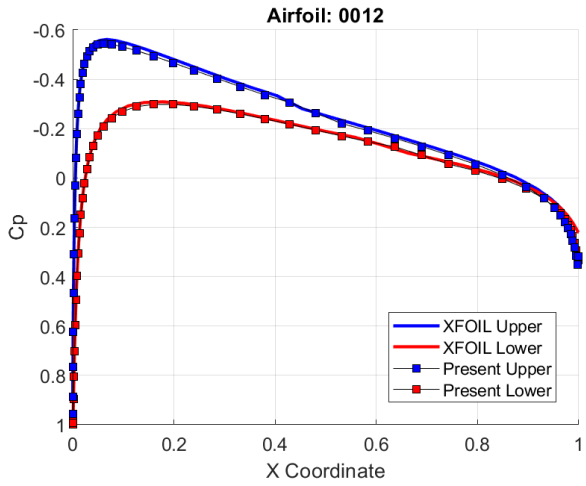

Fig. 26. Pressure Distribution of NACA0012 on Low Angle of Attack

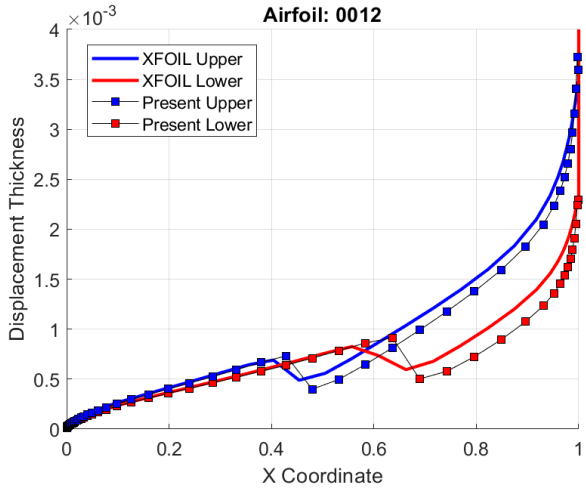

Fig. 27. Displacement Thickness of NACA0012 on Low Angle of Attack

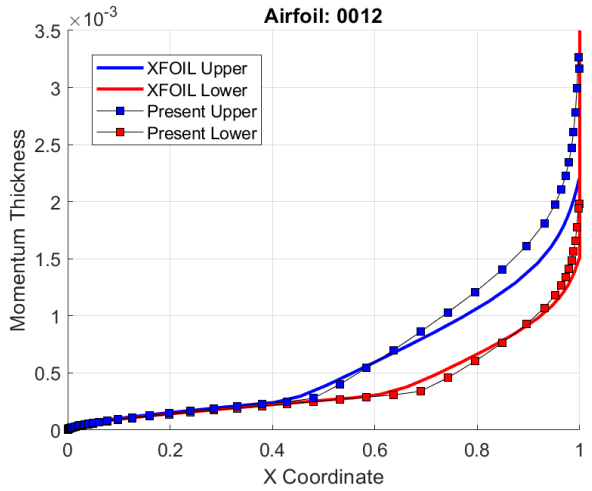

Fig. 28. Momentum Thickness of NACA0012 on Low Angle of Attack

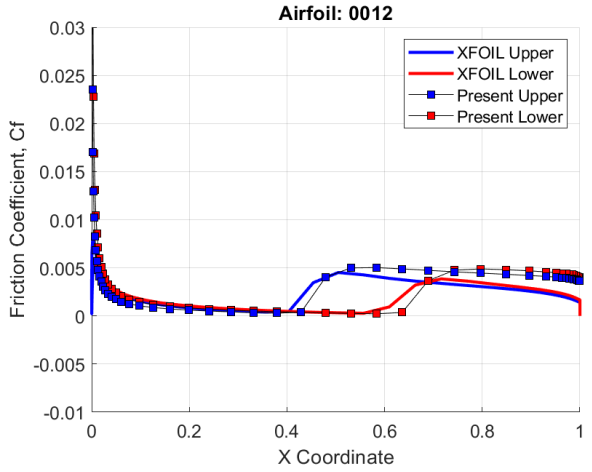

Fig. 29. Friction Coefficient Distribution of NACA0012 on Low Angle of Attack

The comparison of aerodynamic coefficient between present method and XFOIL for low angle of attack case is shown by the table V. For the lift coefficient, the present method is nearly as same as the XFOIL result. However, the present method over predicted the drag coefficient.

TABLE V
AERODYNAMIC COEFFICIENT COMPARISON OF NACA0012 ON LOW ANGLE OF ATTACK

parameters	present	XFOIL	error
lift coefficient, c_l	0.101092	0.112100	9.8%
drag coefficient, c_d	0.007740	0.004980	55.4%

F. High Angle of Attack

Lastly, we validate our solver on high angle of attack condition. The configuration and condition is set as same as the low angle of attack's, the different is the angle of attack is set to 10 deg. The present method can predict accurately the pressure coefficient and displacement thickness as shown on figure 31 and 32, respectively. But, the momentum thickness and the skin friction coefficient are slightly different with the XFOIL result. There reason why it occur is due to flow transition that occur near the leading edge. As we can see from figure 30, the transition is on the upper surface occurs on the leading edge. The Head's method can not analyze accurately the the turbulent boundary layer in this section.

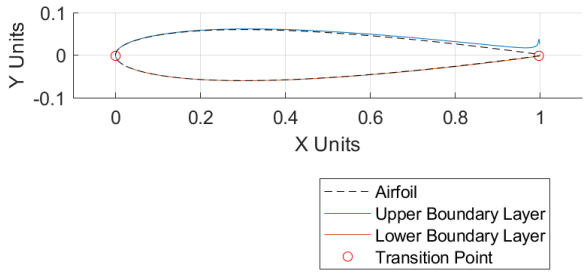

Fig. 30. Boundary Layer Displacement of NACA0012 on High Angle of Attack

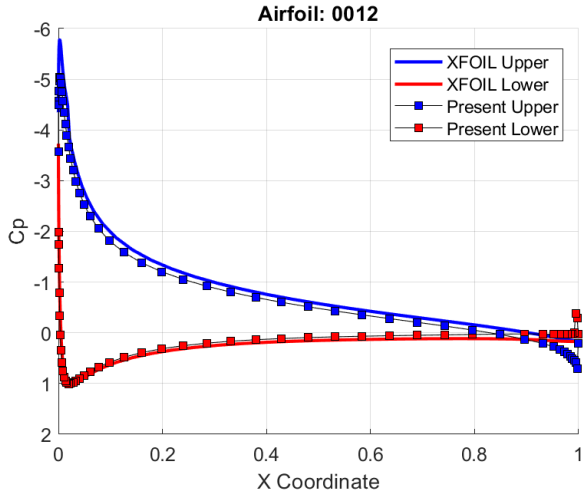

Fig. 31. Pressure Distribution of NACA0012 on High Angle of Attack

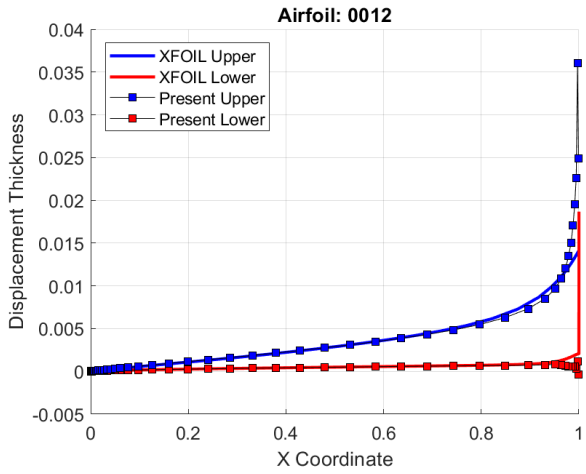

Fig. 32. Displacement Thickness of NACA0012 on High Angle of Attack

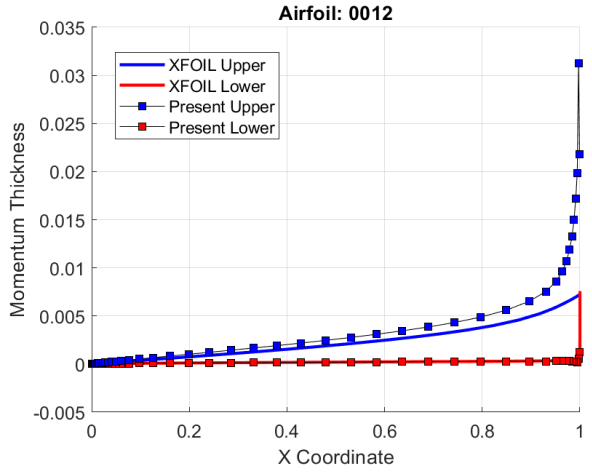

Fig. 33. Momentum Thickness of NACA0012 on High Angle of Attack

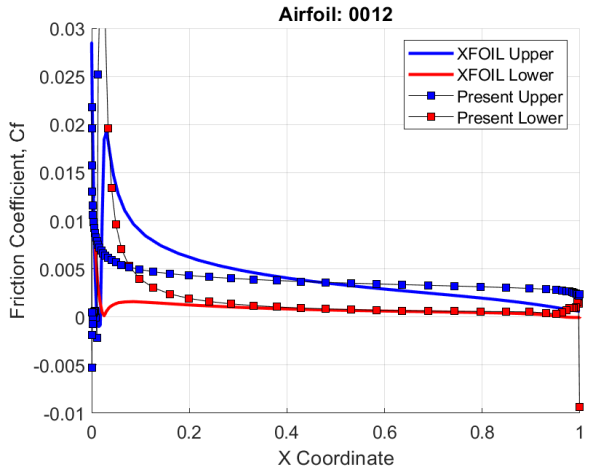

Fig. 34. Friction Coefficient Distribution of NACA0012 on High Angle of Attack

Because of the skin friction coefficient over the airfoil surface can not be predicted accurately by the present method, the resulted drag coefficient is not accurate too, as shown by the table VI below. While, on the other hand, the lift coefficient resulted from the present method is still accurate.

TABLE VI
AERODYNAMIC COEFFICIENT COMPARISON OF NACA0012 ON HIGH ANGLE OF ATTACK

parameters	present	XFOIL	error
lift coefficient, c_l	0.891787	1.122900	20.6%
drag coefficient, c_d	0.159472	0.011020	1347.1%

VII. CONCLUSION

The approximation of boundary layer using both Thwaites method and Head's Entrainment is done in this project. The idea to approximate the boundary layer is by dividing the flow into two regimes: inviscid flow and viscous flow. The panel method is used to analyze the inviscid flow, while Thwaites method is used to analyze the laminar viscous flow and Head's Entrainment method is used to analyze the turbulent boundary layer. The viscous-inviscid interaction method is applied since the displacement of boundary layer affects inviscid flow. The result shows that the present method can predict the boundary layer accurately in the laminar flow regime. The trend of boundary layer displacement thickness and momentum thickness is similar to XFOIL results in the laminar flow regime. Unfortunately, the present method can not predict accurately the boundary layer on high angle of attack condition.

VIII. SOURCE CODE

The source code of the viscous-inviscid interaction made in this project can be accessed in https://github.com/farrasarira/BL-Approximation-using-Thwaites-and-Head-s-Entrainment-Method.

REFERENCES

[1] "Hess-smith panel method." January 2005.
[2] L. Prantd, "Uber flussigkeitsbewegung bei sher kleiner reibung," *Proc. Third Intern. Math. Congress, Heidelberg*, pp. 484–491, 1904.
[3] E. Pohlhausen, "Der wärmeaustausch zwischen festen körpern und flüssigkeiten mit kleiner reibung und kleiner wärmeleitung," *ZAMM-Journal of Applied Mathematics and Mechanics/Zeitschrift für Angewandte Mathematik und Mechanik*, vol. 1, no. 2, pp. 115–121, 1921.
[4] B. Thwaites, "Approximate calculation of the laminar boundary layer," *Aeronautical Quarterly*, vol. 1, no. 3, pp. 245–280, 1949.
[5] H. Thompson, *New Zealanders with the Royal Air Force: Vol. II.* Department of Internal Affairs, 1956.
[6] M. Head, "An approximate method of calculating the laminar boundary layer in two-dimensional incompressible flow," 1957.
[7] M. Head, "Entrainment in the turbulent boundary layer," 1958.
[8] A. E. Veldman, "Entrainment and boundary-layer separation: a modeling history," *Journal of Engineering Mathematics*, vol. 107, no. 1, pp. 5–17, 2017.
[9] B. G. Newman, *Some contributions to the study of the turbulent boundary-layer near separation*. Department of Supply, Aeronautical Research Consultative Committee, 1951.
[10] G. B. Schubauer and P. Klebanoff, "Investigation of separation of the turbulent boundary layer," tech. rep., 1951.
[11] F. M. White and J. Majdalani, *Viscous fluid flow*, vol. 3. McGraw-Hill New York, 2006.

Group Member's Contribution

Initially, the group's workload was divided equally to work on this project. Unfortunately, some of the members are not so active and gives small contribution.

TABLE VII
GROUP MEMBER'S CONTRIBUTION

Name	Contribution
Muhammad Farras Arira	developed source code wrote section II wrote section III wrote section IV wrote section V wrote section VI
Terang B Brantas	wrote section VI
Derren Audric	wrote section VII
Hanna Millah	wrote section I